Materials Science & Engineering C 105 (2019) 110015

Contents lists available at ScienceDirect

Materials Science & Engineering C

journal homepage: www.elsevier.com/locate/msec

Novel porous Ti35Zr28Nb scaffolds fabricated by powder metallurgy with excellent osteointegration ability for bone-tissue engineering applications

Wei Xu[a,1], Jingjing Tian[c,1], Zhuo Liu[b,1], Xin Lu[a,*], Muhammad Dilawer Hayat[d], Yu Yan[a], Zhou Li[b], Xuanhui Qu[a], Cuie Wen[e]

[a] Beijing Advanced Innovation Center for Materials Genome Engineering, Institute for Advanced Materials and Technology, University of Science and Technology Beijing, Beijing 100083, China
[b] CAS Center for Excellence in Nanoscience, Beijing Key Laboratory of Micro-nano Energy and Sensor, Beijing Institute of Nanoenergy and Nanosystems, Chinese Academy of Sciences, Beijing 100083, China
[c] Central Laboratory, Peking Union Medical College Hospital, Peking Union Medical College, Chinese Academy of Medical Sciences, Beijing 100730, China
[d] Department of Chemical and Materials Engineering, University of Auckland, Auckland 1142, New Zealand
[e] School of Engineering, RMIT University, Melbourne 3001, Australia

ARTICLE INFO

Keywords:
Ti35Zr28Nb alloy
Porous scaffolds
Powder metallurgy
Biocompatibility
Osteointegration

ABSTRACT

Titanium (Ti) based porous alloys have been widely used as orthopedic implants. However, the successful applications of these porous Ti alloys need to have the ability to mimic the mechanical properties of natural bone. Novel porous Ti35Zr28Nb scaffolds were fabricated *via* powder metallurgy (PM), and the fabricated scaffold with 61.1% porosity exhibited favorable mechanical properties with a compression yield strength of 132.5 ± 3.5 MPa and an elastic modulus of 2.9 ± 0.4 GPa, which are desired mechanical properties for bone implant material applications. The extracts of the porous Ti35Zr28Nb scaffolds showed no toxic effect on cell proliferation *in vitro* and their cytotoxicity grade was at level 0, similar to that of as-cast pure Ti and Ti-6Al-4 V alloy. Additionally, the extracellular alkaline phosphatase (ALP) level of MC3T3-E1 indicated that the bone matrix synthesis on the porous Ti35Zr28Nb scaffolds was slightly higher than that of as-cast Ti-6Al-4 V and pure Ti alloys. After implantation in rat distal femurs for 8 weeks, the porous Ti35Zr28Nb scaffolds were surrounded by new bone tissue, and the numbers of red blood cells, white blood cells, immunocyte cells, and neutrophil cells returned to the normal levels, which indicate that the porous Ti35Zr28Nb scaffolds possess good *in vivo* osteointegration ability and hemocompatibility. It hence can be concluded that the PM-fabricated Ti35Zr28Nb scaffolds, which have desired mechanical properties and excellent biocompatibility and osteointegration, are a promising candidate alloy for bone-tissue engineering applications in orthopedics.

1. Introduction

Titanium (Ti) and Ti-based alloys have been used extensively for orthopedic and dental implants due to their good mechanical properties, excellent corrosion resistance, and favorable biocompatibility [1–4]. However, the high potential for aseptic loosening of the implants is still a major problem [5]. Clinical practices and studies have proved that the mismatching of the elastic modulus between pure Ti and its alloys (*e.g.*, ~110 GPa for pure Ti and Ti-6Al-4 V) and natural bone (3–30 GPa for cortical bone and 0.02–3 GPa for trabecular or cancellous bone) can lead to stress-shielding and thus causes bone resorption leading to failure of the metallic implant fixtures [6]. In addition, weak interfacial bonding between implants and natural bone, and the lack of biological anchorage for bone-tissue in-growth, are lingering issues that cannot be ignored [7]. Furthermore, releasing of toxic aluminum (Al) and vanadium (V) ions over time for most currently commonly used Ti alloys, such as Ti-6Al-7Nb and Ti-6Al-4V (wt%, hereafter), is causing various diseases, such as Alzheimer's disease and mental disorder [8]. Therefore, developing new Ti alloys with a low elastic modulus that matches native bone, high biocompatibility, and osteointegration ability is an urgent demand for clinical application. Notable examples include TiNbZr [9,10] and TiMo [11,12] base alloys. In particular, TiNbZr alloys containing different levels of niobium (Nb) and zirconium (Zr) have received extensive attention due to the fact that Nb and Zr are not only considered to display excellent biological responses, but can also improve the wear and corrosion properties [13,14].

* Corresponding author.
E-mail address: luxin@ustb.edu.cn (X. Lu).
[1] These authors contributed equally.

https://doi.org/10.1016/j.msec.2019.110015
Received 11 May 2019; Received in revised form 21 July 2019; Accepted 25 July 2019
Available online 26 July 2019

Recently, Wen et al. [15] designed a novel β-Ti35Zr28Nb alloy through the d-electron theory, the molybdenum equivalence (Mo_{eq}), and the electron-to-atom ratio (e/a) approaches. The bulk Ti35Zr28Nb alloy exhibited excellent *in vitro* cytocompatibility and superior mechanical properties [15], although its elastic modulus (64 ± 4.5 GPa) was still at least 2 times higher than that of natural bone (0.02–30 GPa) [15]. In order to match the elastic modulus of Ti35Zr28Nb alloys with that of natural bone, a porous structure was introduced to the alloys. A certain degree of porosity not only reduces the elastic modulus of the alloys, but also leads to tight bonding between the implants and the surrounding bone tissue by allowing new bone-tissue ingrowth [16]. Additionally, the porous structure can provide a pathway for the transport of nutrients and oxygen, which is essential for vascularization during bone-tissue regeneration [17–21]. There are various methods to fabricate porous scaffolds, such as the powder metallurgy (PM) technique using space-holder sintering, foaming, and additive manufacturing (AM) [22–27]. Among them, the PM technique coupled with temporary space-holder sintering is a cost-effective processing method to fabricate porous structures because this method allows flexible adjustment of the composition of the metal powders and does not require expensive equipment [28]. So far, sodium chloride [29], carbamide [30], sugar pellets [31], tapioca [32], saccharose [33], magnesium [34], and ammonium hydrogen carbonate (NH_4HCO_3) [35–40] have been used as space-holder materials. Among these space-holder materials, NH_4HCO_3 is favorable for fabricating porous Ti scaffolds because it has low cost and is easily removed by sintering during the scaffold fabrication.

In this study, Ti35Zr28Nb scaffolds were prepared by the PM technique employing NH_4HCO_3 as the space-holder material. The pore characteristics, matrix phase, mechanical properties, and *in vitro* biocompatibility of the PM-fabricated Ti35Zr28Nb scaffolds. Then the *in vivo* osseointegration of the scaffolds was assessed using a Sprague-Dawley (SD) rat model. This research not only provides a simple manufacturing method for fabricating porous Ti35Zr28Nb scaffolds, but also presents the basic supporting information for their clinical applications as orthopedic implants.

2. Materials and methods

2.1. Materials and specimen fabrication

Atomized Ti28Nb35.4Zr powders (purity ≥ 99.9%, 75 ≤ particle size ≤ 150 μm) was supplied by Wen group (RMIT University, Australia) who fabricated the powders using continuous inert gas atomization method. The powder was milled for 30 min firstly. The frequency of ball milling was 1400 r/min, and the weight ratio of ball to powder was 3:1. The detailed milling process is described in a previous work [41–43]. The SEM micrographs of atomized and ball-milled powders are shown in Fig. 1(a) and (b). Before milling, the powders were typical spherical shape, and the average particles size is 80.5 μm. After milling, the shape of the powders become irregular and the average particles size is 15.2 μm. The as-milled Ti35Zr28Nb powder was then blended with NH_4HCO_3 particles as the space-holder, and the weight ratios were set at 5 levels: 35%, 40%, 45%, 50% and 55%. The optical microscope of NH_4HCO_3 particles are shown in Fig. 1(c) and (d). The NH_4HCO_3 particles have an irregular shape and the size ranged from 180 μm to 250 μm. After blending, the mixtures were cold-pressed at 260 MPa into cylindrical green compacts with dimensions of 15 mm (diameter) × 7 mm (height). Subsequently, the compacts were sintered in a tube furnace under an argon atmosphere. Specimens were initially heated to 1000 °C by 5 °C/min for 2 h, and then heated to 1550 °C at 2 °C/min and held for 2 h. The scaffolds specimens were obtained after the tube furnace was cooled to room temperature.

2.2. Materials properties characterization

The phase identification of the Ti35Zr28Nb scaffolds was performed by X-ray diffraction (XRD) (Dmax-RB X-ray diffractometer, Japan) with Cu Kα radiations. The λ and scan speed were 0.15406 nm and 10°/min, respectively. The pore morphology of the scaffolds was observed by an OLS4000 optical microscope (Japan), and the average pore size was measured using Image-Pro-Plus6 (IPP6) software. The total porosity and open porosity were measured in accordance with the procedures listed in GB/T 5163-2006 and GB/T 5164- 1985 standards[44], respectively, using the following equations:

$$\rho = \frac{m_1}{m_2 - m_3}\rho_1 \tag{1}$$

$$P = \left(1 - \frac{\rho}{\rho_2}\right) \times 100\% \tag{2}$$

where ρ, ρ_1, and ρ_2 are the density of the fabricated alloy (g cm^{-3}), the density of the water (1 g cm^{-3}), and the theoretical density of the alloy (6.36 g cm^{-3}), respectively; m_1, m_2, and m_3 are mass of the alloy in the air (g), the mass of the alloy covered with paraffin in the air (g), and the mass of the alloy covered with paraffin in water (g), respectively; P is the porosity (%). The compressive properties of the fabricated scaffolds with dimensions of 3 mm (diameter) × 5 mm (height) were performed by compression tests, which were carried out on an Instron machine. A strain rate of $2 \times 10^{-3}\,s^{-1}$ was used in the compression tests. The elastic modulus was obtained from the engineering stress-strain curves. For each scaffold, five samples were measured and the average values were obtained.

2.3. In vitro cytocompatibility assay

2.3.1. Cell culture

Murine osteoblast (MC3T3-E1) cells were used to evaluate the *in vitro* cytocompatibility of the Ti35Zr28Nb scaffolds. The as-cast Ti-6Al-4V and pure Ti alloys were selected as controls since they are commonly used for dental and orthopedic implant materials. The cells were cultured in Modified Eagle's Medium (DMEM, Gibco) supplemented with 10% fetal bovine serum (FBS, Gibco) and 1% penicillin/streptomycin in an incubator containing 5% CO_2 at 37 °C.

2.3.2. In vitro osteoblast responses

The extracts were obtained after the specimens were immersed in DMEM for 24 h in an incubator. Then, cells were incubated at a density of 5000 cells per 100 μL by the extracts. At 1 day, 2 days, 3 days, and 7 days, 10 μL MTT solution was added to each well, and incubated for 4 h further. Afterward, the extracts were removed and 100 μL DMSO was added to each well and incubated for 5 min. The optical density (OD) of each well was measured at the wavelength of 570 nm by a multimode detector (BioTek, US). The cell viability ratio (*CVR*) was measured by the following formula:

$$CVR = \left(\frac{OD_{570nm} \text{ in experimental extract}}{OD_{570nm} \text{ in control extract}}\right) \times 100\% \tag{3}$$

The cytotoxicity of the scaffolds was categorized into 6 groups: 0: $CVR \geq 100\%$; 1: $CVR = 75\%–99\%$; 2: $CVR = 50\%–74\%$; 3: $CVR = 25\%-49\%$; 4: $CVR =$: 1%–24%; 5: $CVR \leq 1\%$ based on the ISO 10993-5 [45].

For the cell proliferation observations, sterilized Ti35Zr28Nb scaffolds, as-cast pure Ti, and Ti-6Al-4V alloys were placed in a 24-well plate. Each well was then filled with MC3T3-E1 cells at a density of 1×10^5 cells/mL, and incubated an incubator containing 5% CO_2 at 37 °C for 1, 2, and 3 days, respectively. The cell nuclei and cytoskeleton were stained by DAPI and phalloidin (Sigma), respectively. The images of stained cell nuclei and cytoskeleton were observed by a fluorescence microscope.

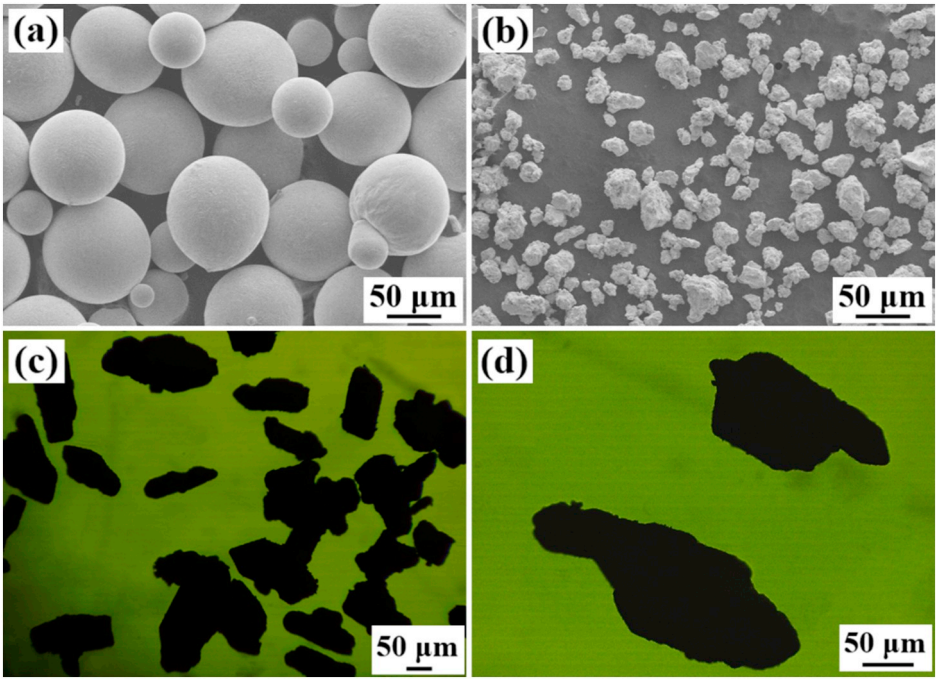

Fig. 1. SEM images of atomized powders (a), ball-milled powders (b), and optical microscope of space-holder (NH_4HCO_3) (c) and (d).

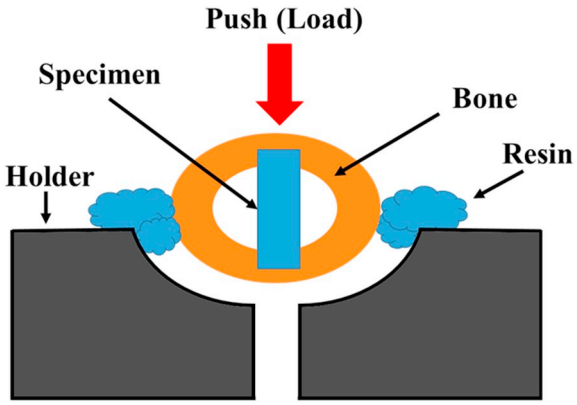

Fig. 2. Diagram of biomechanical test.

The extracellular alkaline phosphatase (ALP) level produced by the MC3T3-E1 cells was measured to obtain the function activity of the cells cultured on each specimen. Cells cultured on each specimen for 1, 3, and 5 days were assessed using an ALP activity kit. The absorbance was measured at 450 nm on an ELISA reader. All cell culture experiments, including indirect testing, direct testing, and extracellular ALP level analysis, were conducted in quintuplicate in order to verify the reproducibility.

2.4. Implantation

2.4.1. Animals

Adult male Sprague-Dawley (SD) rats (200–250 g in weight) were obtained from the Academy of Military Medical Science. The animals were housed under standard conditions at 25 °C. All surgical procedures were performed in a sterile environment at the Beijing Institute of Nanoenergy and Nanosystem. Ethics was approved beforehand by the Animal Research Committee of the Institute.

2.4.2. Surgery

The rats were firstly injected 1% (wt%) pentobarbital solution (Merck, Germany) at a ratio of 10–12.5 mL/kg. Then, the knee joint region was rinsed by iodine and 75% ethanol, respectively, and shaved subsequently. A hole with 1.3 mm diameter was drilled by a hand-drill at the right distal femur, and then Ti35Zr28Nb scaffolds rods (diameter of1.3 ± 0.05 mm and length of 3 ± 0.05 mm, respectively) were pressed into. After surgery, clavulanate-potentiated amoxicillin was injected to each rat for the first 3 days, and no attempts were made to limit their movement. Signs of complications or any other adverse reactions were observed macroscopically.

2.4.3. Blood, micro-CT, histological, and biomechanical analysis

The rats were euthanized at 2, 4, 8 and 16 weeks, and six rats were euthanized at each time point. Before euthanization, blood specimens (0.5 mL) were obtained from the tail vein for complete blood counting. The implant sites were subsequently evaluated macroscopically for hemorrhage and necrosis analyses. Then, six distal pieces of each femur containing the Ti35Zr28Nb scaffold rod were obtained, and examinated by micro-CT (Quantum GX, PerkinElmer).

The bonding strength between the bone and the implant was tested by a biomechanical testing, which was carried out using a specially designed device. As Fig. 2 shown, the obtained block was fixed by resin onto the holder, and the loading directing was parallel to the test specimen. The ross-head speed was 0.5 mm/min. The bonding strength was obtained by load-displacement curves.

The osteointegration ability between the bone and the implant was evaluated by hard-tissue slicing. The specimens were fixed firstly in 10% formalin solution for 2 weeks, and then dried in a graded ethanol series (70% to 100%). Afterwards, the dried specimens were embedded in a methyl methacrylate (MMA) solution without decalcification at 37 °C for 1 week. Finally, the specimens were cut by a diamond saw (Leica) in low speed into 250 μm, and then polished to thickness of ~20 μm. The specimens were stained with toluidine blue. The morphology of new bone was observed by optical microscopy.

2.5. Statistical analysis

The experimental results are expressed as means ± standard deviations. The differences between groups were observed by one-way

Table 1
Impurity levels in Ti35Zr28Nb alloy powder and as-sintered samples (wt%).

Alloy with different NH_4HCO_3 added	Raw powder			As-sintered samples		
	C	N	O	C	N	O
Ti35Zr28Nb (35%)	0.01	0.005	0.09	0.03	0.005	0.15
Ti35Zr28Nb (40%)	0.01	0.005	0.09	0.04	0.006	0.17
Ti35Zr28Nb (45%)	0.01	0.005	0.09	0.03	0.005	0.16
Ti35Zr28Nb (50%)	0.01	0.005	0.09	0.04	0.006	0.15
Ti35Zr28Nb (55%)	0.01	0.005	0.09	0.03	0.006	0.16

analysis of variance (SPSS 14.0 for Windows, SPSS Inc., Chicago, IL) to determine the statistical significance. $P < 0.05$ was considered statistically significant.

3. Results and discussion

3.1. Impurity level, phase identification, pore characteristics, and mechanical properties

Interstitial elements (C, O, N) can markedly affect the mechanical and biocompatible properties of Ti alloys. Table 1 lists the C, O and N contents in the raw powder and sintered samples. It can be seen that both O and C increased slightly after sintered, and the increase in oxygen *vs*. raw powder is 0.07 wt% (sintered in high purity argon). Both increments are limited and typical of PM Ti processes, which indicate that PM is suitable process to fabricate this alloy.

The phase of the porous Ti35Zr28Nb scaffolds with different NH_4HCO_3 weight ratios added were identified by XRD (Fig. 3(a)). It can be seen that the NH_4HCO_3 had no obvious effect on the XRD patterns of the PM-fabricated Ti35Zr28Nb scaffolds. The diffraction peaks of the Ti35Zr28Nb scaffolds indicated that the Ti35Zr28Nb scaffolds were consisted of a single β phase. Fig. 3(b) shows the engineering stress-strain curves of the Ti35Zr28Nb scaffolds with different NH_4HCO_3 weight ratios added. All porous Ti35Zr28Nb scaffolds showed similar stress-strain behaviors and no fracturing occurred on any of the scaffold samples up to 50% strain, indicating excellent elastic-plastic deformation ability.

The micrographs and corresponding pore size distributions of the Ti35Zr28Nb scaffolds with different NH_4HCO_3 weight ratios added are shown in Fig. 3(c–e) and (f–g), respectively, wherein d_{50} represents pore diameters of 50% at cumulative pore sizes (by frequency) and is usually utilized to express the average pore size. It was found that both the porosity and average pore size were increased significantly when the weight ratio of NH_4HCO_3 increased from 35% to 55%.

The pore characteristics and mechanical properties of the Ti35Zr28Nb scaffolds, including porosity, average pore size, compression yield strength, and elastic modulus, are listed in Table 2. It can be seen that, in increasing the NH_4HCO_3 ratio from 35% to 55%, the porosity increased from 51.4% to 64.9%, and the d_{50} increased from 229.9 μm to 427.4 μm. The average pore size increased with increasing the content of NH_4HCO_3 has 2 reasons. The first reason is that with an increase in NH_4HCO_3 there are more NH_4HCO_3 in the alloys and some of the NH_4HCO_3 are connected together, hence the average pore size of the alloys increased with increasing the NH_4HCO_3. In addition, the volume of NH_4HCO_3 will expand during the decomposition, which also increased the average pore size. The compressive yield strength and elastic modulus decreased gradually from 230.5 MPa to 79.7 MPa and from 6.9 GPa to 1.8 GPa, respectively, with porosity increasing from 51.4% to 64.9%.

Whether a scaffold can be used as an orthopedic implant material is determined by the pore characteristics and mechanical properties of the scaffold. In general, pore size between 100 μm and 400 μm is regards as optimal for bone-tissue ingrowth [3,46–49]. With the addition of 35%–55% NH_4HCO_3, the average pore size of the porous Ti35Zr28Nb scaffolds can be regulated ranging from 229.9 μm to 427.4 μm, which is in the desired pore size range for bone tissue ingrowth. Additionally, higher porosity leads to better bone osteointegration performance because the highly porous structure can not only provide more places for bone to grow but also has a higher surface area for cell adhesion and proliferation. However, an increase in porosity decreases inevitably the strength of the scaffolds. With the increase in porosity, the compression yield strength of the alloy ranged from 230 MPa to 80 MPa. Compared with the pure Ti and Ti-6Al-4 V with similar porosity, the porous Ti35Zr28Nb scaffold exhibited higher strength than pure Ti and similar strength to the Ti-6Al-4 V (Table 2). In addition, the porous Ti35Zr28Nb scaffold fabricated by PM in this study also presented higher strength than SLM-fabricated porous Ti35Zr28Nb scaffold in similar porosity.

As reported [6], the compressive yield strength and elastic modulus of human trabecular or cancellous bone in the range of 2–80 MPa and 0.02–3.0 GPa, respectively. The porous Ti35Zr28Nb scaffold with 61.1% porosity exhibited a compressive yield strength of 132.5 MPa, a strength higher than that of cancellous bone and which can be assumed to provide adequate mechanical support to host bone tissue, and an elastic modulus of 2.9 GPa, an elastic modulus closes to that of cancellous bone and which can be anticipated to minimize or eliminate the stress-shielding effect. Therefore, the porous Ti35Zr28Nb scaffold with 61.1% porosity can be anticipated to be a promising candidate implant material. Hence, the biocompatibility and osteointegration assessment were focused on the Ti35Zr28Nb scaffold with 61.1% porosity.

3.2. In vitro cytocompatibility

The cytotoxicity of the extracts of the porous Ti35Zr28Nb scaffolds was assessed using MTT assay and the results are shown in Fig. 4(a). As-cast pure Ti and Ti-6Al-4 V alloys were tested for comparison, and cells cultured in DMEM were used as a positive control. As Fig. 4(a) shown, the MC3T3-E1 cells cultured using the porous Ti35Zr28Nb scaffold extract showed similar cell viability to that of the cells cultured using extracts from the as-cast Ti-6Al-4 V and pure Ti alloys at different time points. Based on ISO 10993-5 [45], the cytotoxicity level for the Ti35Zr28Nb scaffold, as-cast pure Ti, and Ti-6Al-4 V is at level 0, indicating no adverse effect for MC3T3-E1 cells.

The ALP level, which indicates the function activity of the MC3T3-E1 cells, including the beginning of bone matrix synthesis and the maturity of the extracellular matrix[50–53], is tested (Fig. 4(b)). It can be seen that, with increasing culture time, the OD value for all the sample groups increased significantly, indicating that the amount of bone matrix increased. Compared with the as-cast pure Ti and Ti-6Al-4V groups, the porous Ti35Zr28Nb scaffold group showed a slightly higher OD value at each time point, which implies that the amount of bone matrix was higher on the Ti35Zr28Nb scaffold. However, the differences among the different groups at each time point are not statistically significant ($P > 0.05$). This result indicates that all the four groups of samples have good cytocompatibility and can promote the proliferation of MC3T3-E1 cells.

Fig. 5 shows the morphology of the MC3T3-E1 cells cultured on the surface of Ti35Zr28Nb scaffold, as-cast Ti-6Al-4V, and pure Ti alloys for up to 3 days. The cytoskeleton structure (green in color) among the three groups of samples at each measuring time point has no significant difference. Moreover, the number of nuclei (blue) increased with culture time significantly for each group. After cell culturing for 3 days, the cell number on the surface of the porous Ti35Zr28Nb scaffold was greater than for the cells cultured on the as-cast pure Ti and Ti-6Al-4V, indicating that the porous structure may have promoted cell growth and proliferation. These results further confirm the excellent *in vitro* cytocompatibility of the porous Ti35Zr28Nb scaffolds.

The porous structure, corrosion resistance, and alloying elements are three factors that affect the *in vitro* cytocompatibility of an implant material [54]. In this study, Nb and Zr elements were selected as the alloying elements, as they are reported to display excellent biological

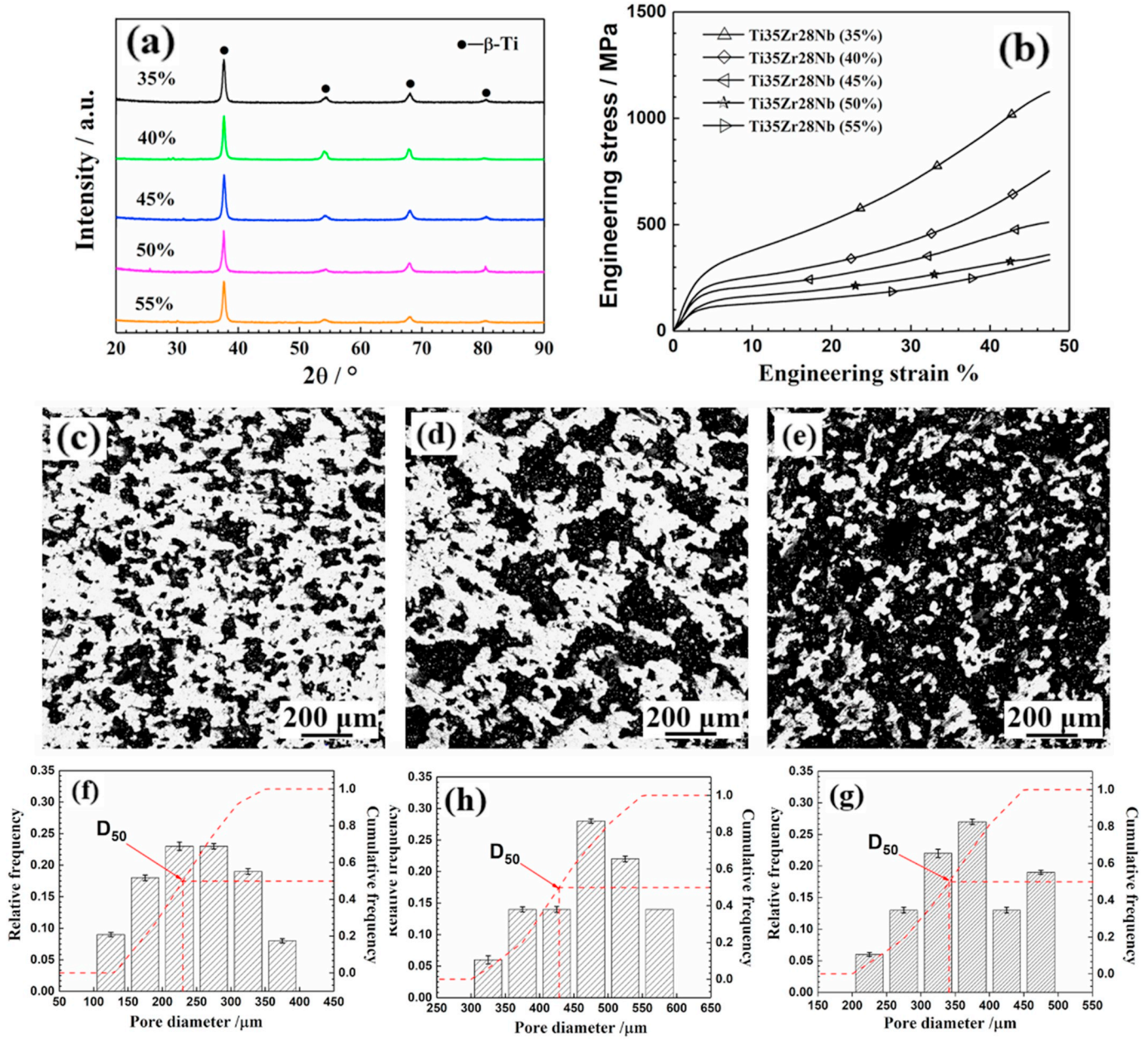

Fig. 3. (a) XRD patterns; (b) engineering stress-strain curves; (c–e) micrographs and (f–g) corresponding pore size distribution of PM-fabricated porous Ti35Zr28Nb scaffolds with different NH_4HCO_3 weight ratios added: (c, f) 35%; (d, h) 45%; (e, g) 55%.

responses [55]. Hence, it is not surprising that the porous Ti35Zr28Nb scaffold showed no cytotoxicity to the MC3T3-E1 cells in the context of these alloying elements. In addition, as reported [13,56,57], due to the spontaneous formation of a stable TiO_2-Nb_2O_5-ZrO_2 passive film, the corrosion resistance of TiNbZr alloy is higher than that of as-cast pure Ti and Ti-6Al-4V alloys. This spontaneously formed oxide film can inhibit the release of metal ions, and hence can reduce the cytotoxicity to cells. Moreover, the porous structure plays a pivotal role in determining the interaction between the implant material and its surrounding tissue. It has been reported that a biological material must provide adequate surface area and internal space for cells to adhere and proliferate [58,59], and for the formation and deposition of

Table 2
Pore characteristics and mechanical properties of Ti35Zr28Nb alloy scaffolds with different NH_4HCO_3 weight ratios added, pure Ti, Ti-6Al-4V, and SLM-fabricated Ti35Zr28Nb.

Alloys	Ti35Zr28Nb (this study)					CP Ti [71]	Ti-6Al-4V [72]	Ti35Zr28Nb [73]
NH_4HCO_3 content (wt%)	35	40	45	50	55	–	–	–
Porosity (%)	51.4 ± 1.1	55.9 ± 1.2	58.8 ± 1.4	61.1 ± 1.5	64.9 ± 1.6	37	56.2 ± 0.4	49.9 ± 3.2
Average pore size (μm)	229.9 ± 5.6	276.2 ± 3.7	341.5 ± 5.7	379.1 ± 7.8	427.4 ± 10.1	–	801 ± 33	–
Compression yield strength (MPa)	230.5 ± 7.6	186.3 ± 7.1	161.6 ± 4.9	132.5 ± 3.5	79.7 ± 3.5	113 ± 6	194.8 ± 1.3	58 ± 3
Elastic modulus (GPa)	6.9 ± 0.6	5.1 ± 0.5	3.9 ± 0.3	2.9 ± 0.4	1.8 ± 0.5	13 ± 3	5.04 ± 0.15	1.3 ± 0.1

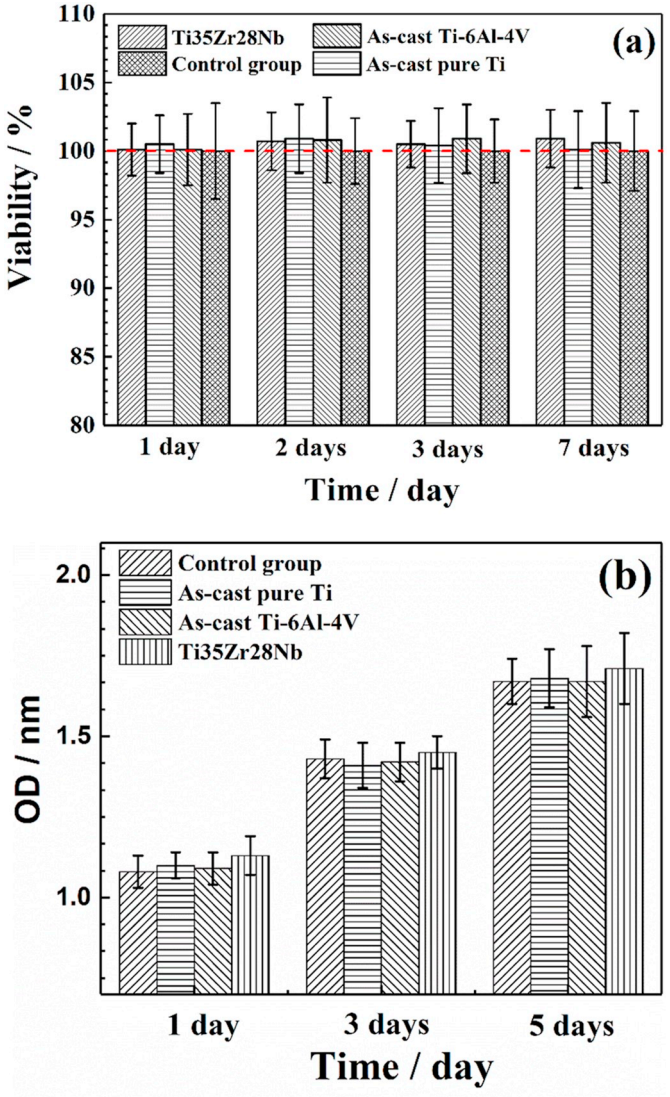

Fig. 4. (a) Effect of extracts of porous Ti35Zr28Nb, as-cast pure Ti, and Ti-6Al-4V alloy on viability of MC3T3-E1 cells at specific time points of 1, 2, 3, and 7 days, $P > 0.05$, $n = 5$. (b) ALP levels of porous Ti35Zr28Nb, as-cast pure Ti, and Ti-6Al-4 V alloy at specific time points of 1, 3 and 5 days, $P > 0.05$, $n = 5$.

extracellular matrix [60,61]. In this study, the porous Ti35Zr28Nb scaffold exhibited a three-dimensional porous structure with an average pore size of 379.1 μm, which provided sufficient space for cell adhesion and proliferation. Therefore, the porous Ti35Zr28Nb scaffold with 61.1% porosity showed excellent *in vitro* cytocompatibility to MC3T3-E1 cells.

3.3. *In vivo* biocompatibility and osseointegration

All the animals recovered after surgery with no postoperative morbidity observed. Fig. 6 shows the implant position, the appearance after surgery, the healing progress of the skin, and the interface between the bone and implant after 2 weeks' implantation. As Fig. 6 had shown, no infections occurred on the implant sites, and new hair grew gradually with prolongation of implantation time. In addition, no intolerant macroscopic signs were observed in terms of hemorrhage or necrosis at any time of implantation, as exemplified by the interface between the bone and implant after 2 weeks implantation (Fig. 6(g)).

Blood analysis was performed at 0, 2, 4, 8 and 16 weeks in order to observe the body systemic responses. The red blood cells, white blood cells, immunocyte cells, and neutrophil cells counts are shown in Fig. 7. It can be seen that no hemolysis occurred after implantation, since the number of red blood cells did not change significantly throughout the implantation period ($P > 0.05$). In addition, it is noted that the number of white blood cell increased slightly in the first 4 weeks after implantation, indicating the occurrence of a mild inflammatory response due to the implantation of large implants. After 8 weeks, the number of white blood cells began to decrease, suggesting the inflammation had mainly subsided. Similar to the white blood cells, the numbers of immunocyte and neutrophil cells, which are biomarkers of physiological stress [62], also increased slightly, which could be related to the larger volume of implant that stretched the muscle. However, there is no significant difference ($P > 0.05$) in the number of white blood cells, immunocyte, and neutrophil cells throughout the course of implantation. These results indicate that the porous Ti35Zr28Nb scaffold possesses good *in vivo* hemocompatibility.

Micro-CT and histological section analysis were performed on the porous Ti35Zr28Nb scaffolds with 61.1% porosity after 2, 4, 8, and 16 weeks of implantation to study the interaction between the bone tissue and the implant. High-resolution micro-CT images are shown in Fig. 8(a–d). It can be seen that new bone started to grow on the implant surface after 2 weeks' implantation (Fig. 8(a)), and eventually, after 8 weeks implantation, the implant was surrounded by new bone (Fig. 8(c)). The amount of new bone at 16 weeks (Fig. 8(d)) was not significantly different from that at 8 weeks, which indicates after 8 weeks' implantation the new bone regeneration has almost completed. Fig. 8(e–h) shows the images of histological sections. As Fig. 8(e) shown, a gap between the Ti35Zr28Nb scaffolds and bone was observed at 2 weeks of implantation, and there was a small osteoid-like new bone formed in the pores of the Ti35Zr28Nb scaffolds. With implantation time passing, the gap decreased gradually and new bone began to form in the porous structure. When the implantation time reached 8 weeks, the gap had disappeared and the porous structure was filled with new bone. Similar to the micro-CT results, the formation of new bone at 16 weeks was not significantly different from that at 8 weeks.

Push-out testing was used to further assess the bone-tissue integration, and Fig. 9 shows the load-displacement curves. As Fig. 9 shown, the bonding strength increased gradually with the extension of implantation time. At 2 weeks, the bonding strength was 61.4 N. When the implantation time increased to 8 weeks, the bonding strength reached 147.5 N. However, at 16 weeks there was only a slight increase in the bonding strength, *i.e.*, an increase of 16.8 N (bonding strength of 164.3 N at 16 weeks), which indicates that new bone regeneration was nearly complete at 8 weeks after implantation. This result is in agreement with the micro-CT and histological results. It was reported that a dense Ti-6Al-4 V alloy requires 24 weeks to complete new bone regeneration [63], while in this study only 8 weeks were needed for the porous Ti35Zr28Nb scaffold to complete new bone regeneration. It can be concluded that the porous Ti35Zr28Nb scaffold has superior osteogenic ability. This may be mainly attributable to the ability of the porous structure of the Ti35Zr28Nb scaffold to provide more space for surrounding bone tissues to anchor [64].

Recently, porous metal materials have received increasing attention due to their excellent biological properties. In this study, the *in vivo* experiment demonstrated that no obvious inflammatory reaction occurred in the vicinity of the porous Ti35Zr28Nb implants (Fig. 4). The blood analysis showed that there was no significant change in the red blood cells throughout the implantation period ($P > 0.05$), which means that no hemolysis occurred after implantation. In addition, the number of white blood cells, immunocyte cells, and neutrophil cells increased slightly in the early weeks of implanting, indicating mild inflammatory and physiological stress. However, after 8 weeks of implantation the number of white blood cells, immunocyte cells, and neutrophil cells returned to normal, suggesting that the inflammatory and physiological stress no longer existed. The micro-CT, histological, and biomechanical results demonstrate that new bone began to grow on the implant surface at 2 weeks and the gap was eventually bridged at

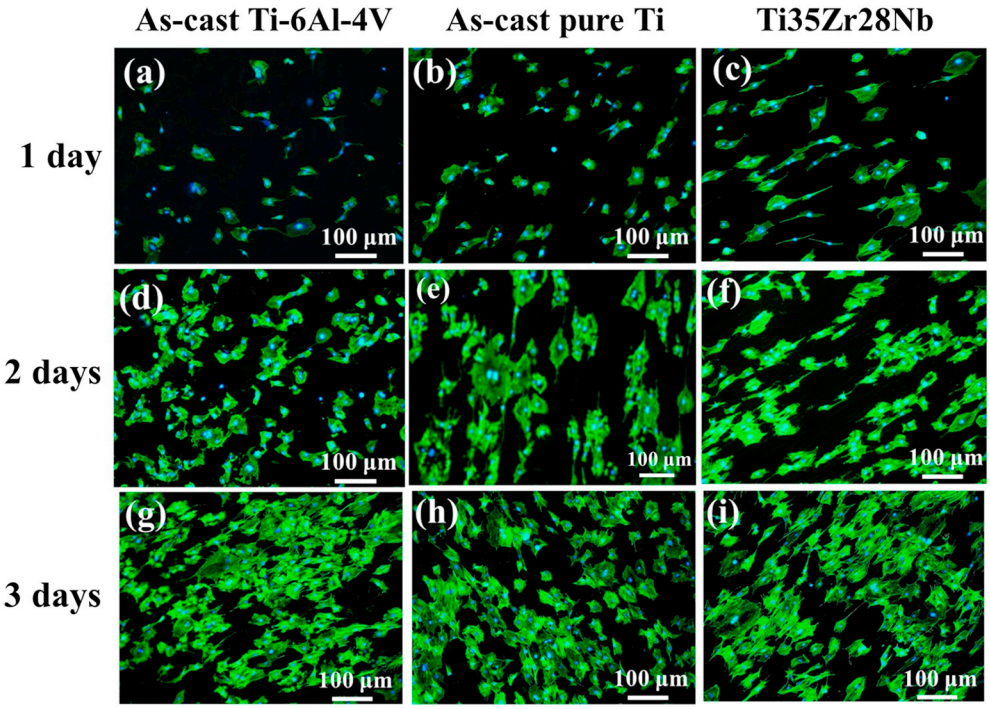

Fig. 5. Morphology of MC3T3-E1 cultured on Ti35Zr28Nb scaffold with 61.1% porosity, as-cast pure Ti, and Ti-6Al-4 V at different time points. Note: cell cytoskeleton (green) and nuclei (blue) were stained by phalloidin and DAPI, respectively. (For interpretation of the references to color in this figure legend, the reader is referred to the web version of this article.)

8 weeks, proving the excellent osteointegration of the Ti35Zr28Nb scaffolds.

The excellent biocompatibility and osteointegration of the Ti35Zr28Nb scaffolds can be linked to the following factors: (1) biocompatible alloying elements added into the alloy; (2) low elastic modulus; and (3) porous structure. It has been reported that the biocompatibility of Nb and Zr is higher than that of Ti [54]. Hence, the additions of Nb and Zr to Ti can further enhance the biocompatibility of the Ti35Zr28Nb alloy. In addition, as reported, low elastic modulus of the implant boosts new bone formation [65]. In the present study, the porous Ti35Zr28Nb scaffold with 61.1% porosity has an elastic modulus about 2.9 GPa, which is lower than that of bulk Ti alloys reported in the literature (*e.g.* ~70 GPa for bulk Ti-13Nb-13Zr [66], and ~110 GPa for bulk Ti-6Al-4 V and pure Ti) significantly. Hence, the he porous Ti35Zr28Nb scaffolds exhibit better osteointegration ability, which is in good agreement with the results reported by Li [67], Wauthle [68], Haugen [69], and Chang [70], who demonstrated that new bone formation in porous alloys or around bulk alloys with lower elastic modulus was faster than with higher elastic modulus. Furthermore, high porosity allows more body fluids to transport, which hence accelerates the healing process. As a result, the porous Ti35Zr28Nb scaffolds fabricated by PM in this study exhibited excellent biocompatibility and osteointegration. These properties together with the simple fabrication method (PM), make these porous Ti35Zr28Nb scaffolds an attractive choice as an orthopedic implant alloy for bone-tissue engineering.

4. Conclusions

(1) Novel porous Ti35Zr28Nb scaffolds with porosity ranging from

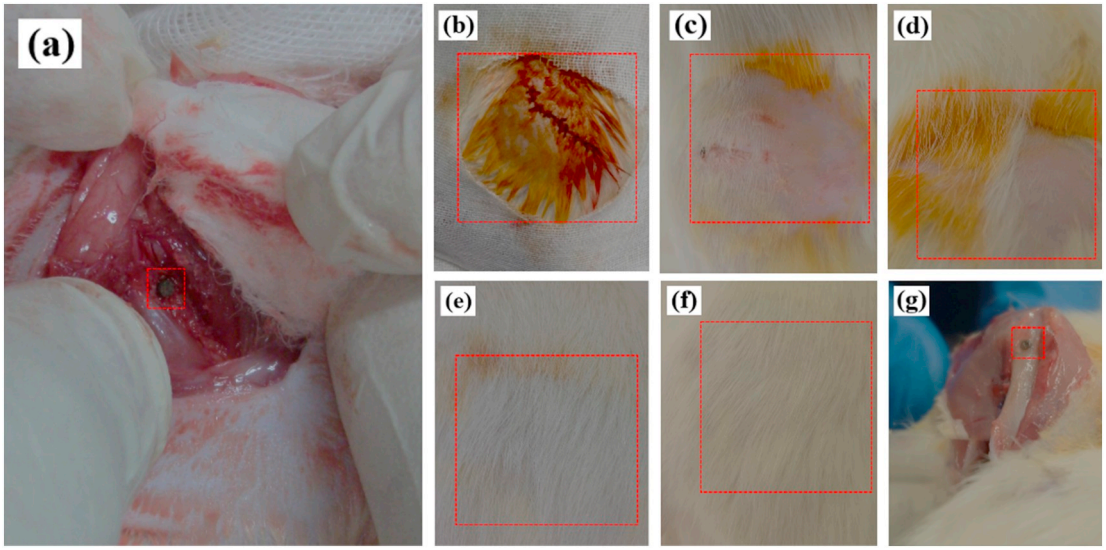

Fig. 6. (a) Implant position; (b) appearance after surgery; (c) 2 weeks post implantation; (d) 4 weeks post implantation; (e) 8 weeks post implantation; (f) 16 weeks post implantation; and (g) interface between bone and implant 2 weeks post implantation.

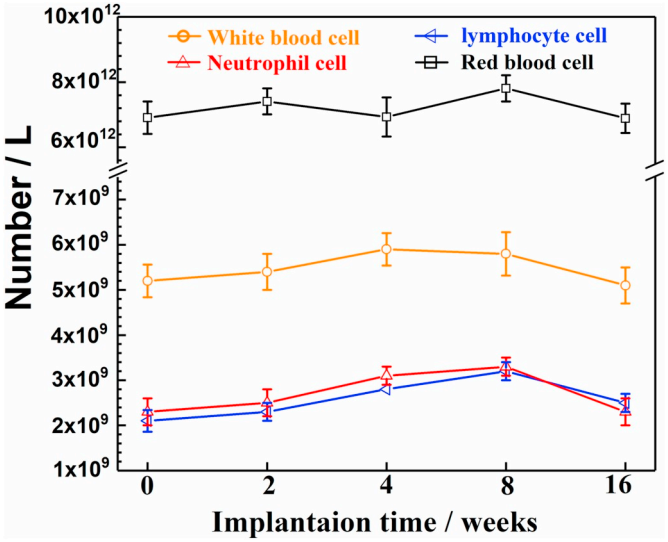

Fig. 7. Numbers of white blood cells, red blood cells, lymphocyte cells, and neutrophil cells after implantation for different numbers of weeks, P > 0.05, n = 6. (For interpretation of the references to color in this figure legend, the reader is referred to the web version of this article.)

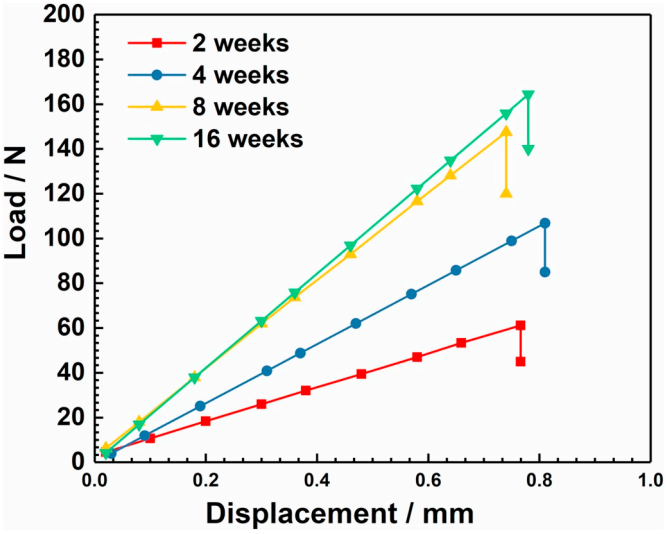

Fig. 9. Peak loads of push-out testing at different implantation time points.

~50% to ~65% and pore size from ~230 μm to ~430 μm were fabricated *via* powder metallurgy. By controlling the NH_4HCO_3 contents, Ti35Zr28Nb scaffolds with different porosities and therefore a wide range of mechanical properties were fabricated. The elastic modulus and the compression yield strength of the scaffolds ranged from 1.8 to 6.9 GPa and 79.7 to 230.5 MPa, respectively.

(2) The extracts of the porous Ti35Zr28Nb scaffolds showed no cytotoxic effects on MC3T3-E1 cells, and the cytotoxicity level was ranked at grade 0. Extracellular ALP analysis showed that the porous Ti35Zr28Nb scaffolds showed excellent osteogenesis ability for MC3T3-E1 cells.

(3) After 8 weeks of implantation in rat distal femurs, the number of red blood cells, white blood cells, immunocyte cells, and neutrophil cells returned to normal, indicating the porous Ti35Zr28Nb scaffolds possess good *in vivo* hemocompatibility. Additionally, the implant was almost entirely surrounded by new bone tissue after 8 weeks of implantation, indicating the excellent osteointegration ability of the Ti35Zr28Nb scaffolds.

(4) This porous Ti35Zr28Nb scaffold fabricated by PM is a promising orthopedic implant material for bone-tissue engineering by virtue of its simple fabrication method, bone-mimicking mechanical properties, and excellent biocompatibility and osteointegration performance.

Data availability

The data that support the findings of this study are available from the corresponding authors on reasonable request.

Declaration of Competing Interest

The authors declare that they have no known competing financial interests or personal relationships that could have appeared to influence the work reported in this paper.

Acknowledgments

This research work is supported by the National Natural Science Foundation of China (51874037) and 13th Five-Year Weapons Innovation Foundation of China (6141B012807). CW acknowledges the financial support for this research by the National Health and Medical Research Council (NHMRC), Australia through project grant (GNT1087290).

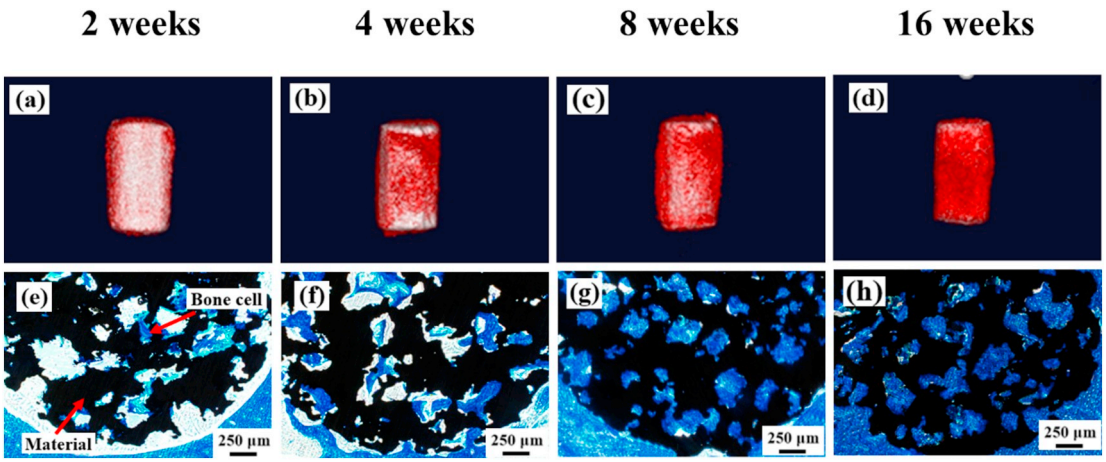

Fig. 8. Micro-CT images and histological sections of porous Ti35Zr28Nb scaffold with 61.1% porosity at different implantation time points.

References

[1] M. Geetha, A.K. Singh, R. Asokamani, A.K. Gogia, Ti based biomaterials, the ultimate choice for orthopaedic implants—a review, Prog. Mater. Sci. 54 (2009) 397–425.

[2] M. Long, H.J. Rack, Titanium alloys in total joint replacement—a materials science perspective, Biomaterials 19 (1998) 1621–1639.

[3] G.E. Ryan, A.S. Pandit, D.P. Apatsidis, Porous titanium scaffolds fabricated using a rapid prototyping and powder metallurgy technique, Biomaterials 29 (2008) 3625–3635.

[4] M. Niinomi, M. Nakai, J. Hieda, Development of new metallic alloys for biomedical applications, Acta Biomater. 8 (2012) 3888–3903.

[5] Y.S. Amin, D.S.J. Van, Y.C. Chai, R. Wauthle, B.Z. Tahmasebi, P. Habibovic, M. Mulier, J. Schrooten, H. Weinans, A.A. Zadpoor, Bone regeneration performance of surface-treated porous titanium, Biomaterials 35 (2014) 6172–6181.

[6] H. Kröger, P. Venesmaa, J. Jurvelin, H. Miettinen, O. Suomalainen, E. Alhava, Bone density at the proximal femur after total hip arthroplasty, Clin. Orthop. Relat. R. 352 (1998) 66–74.

[7] W. Mróz, B. Budner, R. Syroka, K. Niedzielski, G. Golański, A. Slósarczyk, D. Schwarze, T.E. Douglas, In vivo implantation of porous titanium alloy implants coated with magnesium-doped octacalcium phosphate and hydroxyapatite thin films using pulsed laser deposition, J. Biomed. Mater. Res. B 103 (2015) 151–158.

[8] B. Aksakal, O.S. Yildirim, H. Gul, Metallurgical failure analysis of various implant materials used in orthopedic applications, J. Fail. Anal. Prev. 4 (2004) 17–23.

[9] L.M. Elias, S.G. Schneider, S. Schneider, H.M. Silva, F. Malvisi, Microstructural and mechanical characterization of biomedical Ti-Nb-Zr(-Ta) alloys, Mater. Sci. Eng. A 432 (2006) 108–112.

[10] S.J. Li, R. Yang, S. Li, Y.L. Hao, Y.Y. Cui, M. Niinormi, Z.X. Guo, Wear characteristics of Ti-Nb-Ta-Zr and Ti-6Al-4V alloys for biomedical applications, Wear 257 (2004) 869–876.

[11] W. Xu, X. Lu, L.N. Wang, Z.M. Shi, S.M. Lv, M. Qian, X.H. Qu, Mechanical properties, in vitro corrosion resistance and biocompatibility of metal injection molded Ti-12Mo alloy for dental applications, J. Mech. Behav. Biomed. Mater. 88 (2018) 534–547.

[12] W. Xu, Z. Liu, X. Lu, J.J. Tian, G. Chen, B.W. Liu, Z. Li, X.H. Qu, C.E. Wen, Porous Ti-10Mo alloy fabricated by powder metallurgy for promoting bone regeneration, Sci. China Mater. 62 (2019) 1053–1064.

[13] L.T. Duarte, S.R. Biaggio, R.C. Rocha-Filho, N. Bocchi, Surface characterization of oxides grown on the Ti-13Nb-13Zr alloy and their corrosion protection, Corros. Sci. 72 (2013) 35–40.

[14] P. Majumdar, S.B. Singh, M. Chakraborty, Wear response of heat-treated Ti-13Zr-13Nb alloy in dry condition and simulated body fluid, Wear 264 (2008) 1015–1025.

[15] S. Ozan, J. Lin, Y. Li, R. Ipek, C.E. Wen, Development of Ti-Nb-Zr alloys with high elastic admissible strain for temporary orthopedic devices, Acta Biomater. 20 (2015) 176–187.

[16] E. Yılmaz, A. Gökçe, F. Findik, H.O. Gülsoy, O. İyibilgin, Mechanical properties and electrochemical behavior of porous Ti-Nb biomaterials, J. Mech. Behav. Biomed. 87 (2018) 59–67.

[17] S. Sose, M. Roy, A. Bandyopadhyay, Recent advances in bone tissue engineering scaffolds, Trends Biotechnol. 30 (2012) 546–554.

[18] J. Van den Dolder, E. Farber, P.H.M. Spauwen, J.A. Jansen, Bone tissue reconstruction using titanium fiber mesh combined with rat bone marrow stromal cells, Biomaterials 24 (2003) 1745–1750.

[19] E. Marin, S. Fusi, M. Pressacco, L. Paussa, L. Fedrizzi, Characterization of cellular solids in Ti-6Al-4V for orthopaedic implant applications: trabecular titanium, J. Mech. Behav. Biomed. 3 (2010) 373–381.

[20] L.D. Zardiackas, L.D. Dillon, D.W. Mitchell, L.A. Nunnery, R. Poggie, Structure, metallurgy, and mechanical properties of a porous tantalum foam, J. Biomed. Mater. Res. A 58 (2001) 180–187.

[21] Z.F. Guo, Q.Y. Li, F. He, Y. Huang, Y.Z. Wan, Mechanical modulation and bioactive surface modification of porous Ti-10Mo alloy for bone implants, Mater. Design 42 (2012) 13–20.

[22] W. Xu, X. Lu, B. Zhang, C.C. Liu, S.M. Lv, S.D. Yang, X.H. Qu, Effects of porosity on mechanical properties and corrosion resistances of PM-fabricated porous Ti-10Mo alloy, Metals 8 (2018) 188–201.

[23] C.L. Wang, H.J. Chen, X.D. Zhu, Z.W. Xiao, K. Zhang, X.D. Zhang, An improved polymeric sponge replication method for biomedical porous titanium scaffolds, Mater. Sci. Eng. C 70 (2017) 1192–1199.

[24] H.Y. Mi, X. Jing, G. Yilmaz, B.S. Hagerty, E. Enriquez, L.S. Turng, In situ synthesis of polyurethane scaffolds with tunable properties by controlled crosslinking of triblock copolymer and polycaprolactone triol for tissue regeneration, Chem. Eng. J. 348 (2018) 786–798.

[25] S.Y. Chen, J.C. Huang, C.T. Pan, C.H. Lin, T.L. Yang, Y.S. Huang, C.H. Ou, L.Y. Chen, D.Y. Lin, H.K. Lin, T.H. Li, J.S.C. Jang, C.C. Yang, Microstructure and mechanical properties of open-cell porous Ti-6Al-4V fabricated by selective laser melting, J. Alloy. Comp. 713 (2017) 248–254.

[26] H.Y. Mi, M.R. Salick, X. Jing, B.R. Jacques, W.C. Crone, X.F. Peng, L.S. Turng, Characterization of thermoplastic polyurethane/polylactic acid (TPU/PLA) tissue engineering scaffolds fabricated by microcellular injection molding, Mater. Sci. Eng. C 33 (2013) 4767–4776.

[27] G. Engin, B. Aydemir, H.O. Gülsoy, Injection molding of micro-porous titanium alloy with space holder technique, Rare Metals 30 (2011) 565–571.

[28] R.M. Gernman, Progress in titanium metal powder injection molding, Materials 6 (2013) 3641–3662.

[29] Y. Torres, J.J. Pavón, J.A. Rodríguez, Processing and characterization of porous titanium for implants by using NaCl as space holder, J. Mater. Process. Tech. 212 (2012) 1061–1069.

[30] O. Smorygo, A. Marukovich, V. Mikutski, A.A. Gokhale, G. JaganReddy, J. VinodKumar, High-porosity titanium foams by powder coated space holder compaction method, Mater. Lett. 83 (2012) 17–19.

[31] Y.H. Chen, D. Kent, M. Bermingham, A. Dehghan-Manshadi, M. Dargusch, Manufacturing of biocompatible porous titanium scaffolds using a novel spherical sugar pellet space holder, Mater. Lett. 195 (2017) 92–95.

[32] A. Mansourighasri, N. Muhamad, A.B. Sulong, Processing titanium foams using tapioca starch as a space holder, J. Mater. Process. Tech. 212 (2012) 83–89.

[33] J. Jakubowicz, G. Adamek, K. Pałka, D. Andrzejewski, Micro-CT analysis and mechanical properties of Ti spherical and polyhedral void composites made with saccharose as a space holder material, Mater. Charact. 100 (2015) 13–20.

[34] Y.H. Chen, J.E. Frith, A. Dehghanmanshadi, H. Attar, D. Kent, N.D.M. Soro, M.J. Bermingham, M.S. Dargusch, Mechanical properties and biocompatibility of porous titanium scaffolds for bone tissue engineering, J. Mech. Behav. Biomed. Mater. 75 (2017) 169–174.

[35] X.J. Wang, Y.C. Li, J.Y. Xiong, P.D. Hodgson, C.E. Wen, Porous TiNbZr alloy scaffolds for biomedical applications, Acta Biomater. 5 (2009) 3616–3624.

[36] A. Ibrahim, F.M. Zhang, E. Otterstein, E. Burkel, Processing of porous Ti and Ti5Mn foams by spark plasma sintering, Mater. Design 32 (2011) 146–153.

[37] C.E. Wen, Y. Yamada, K. Shimojima, Y. Chino, T. Asahina, M. Mabuchi, Processing and mechanical properties of autogenous titanium implant materials, J. Mater. Sci.: Mater. M. 13 (2002) 397–401.

[38] A.E. Aguilar Maya, D.R. Grana, A. Hazarabedian, G.A. Kokubu, M.I. Luppo, G. Vigna, Zr-Ti-Nb porous alloys for biomedical application, Mater. Sci. Eng. C 32 (2012) 321–329.

[39] H.C. Hsu, S.C. W, S.K. Hsu, M.S. Tsai, T.Y. Chang, W.F. Ho, Processing and mechanical properties of porous Ti-7.5Mo alloy, Mater. Design 47 (2013) 21–26.

[40] A. Nouri, P.D. Hodgson, C.E. Wen, Effect of process control agent on the porous structure and mechanical properties of a biomedical Ti-Sn-Nb alloy produced by powder metallurgy, Acta Biomater. 6 (2010) 1630–1639.

[41] W. Xu, M. Li, C.E. Wen, S.M. Lv, C.C. Liu, X. Lu, X.H. Qu, The mechanical properties and in vitro biocompatibility of pm-fabricated Ti-28Nb-35.Zr alloy for orthopedic implant applications, Materials 11 (2018) 531–543.

[42] W. Xu, S.Q. Xiao, X. Lu, G. Chen, C.C. Liu, X.H. Qu, Fabrication of commercial pure Ti by selective laser melting using hydride-dehydride titanium powders treated by ball milling, J. Mater. Sci. Technol. 35 (2019) 322–327.

[43] W. Xu, X. Lu, M.D. Hayat, J.J. Tian, C. Huang, M. Chen, X.H. Qu, C.E Wen, Pore characteristics, mechanical properties, and corrosion resistance of newly developed porous Ti35Zr28Nb scaffolds fabricated by powder metallurgy for bone-tissue engineering, J. Mater. Res. Technol. doi:https://doi.org/10.1016/j.jmrt.2019.06.021.

[44] GB/T 5163, Sintered Metal Materials, Excluding Hardmetals-permeable Sintered Metal Materials-determination of Density, Oil Content, and Open Porosity, (2006).

[45] ISO 10993-5, Biological Evaluation of Medical Devices-Part 5: Tests for Cytotoxicity: In Vitro Methods, ANSI/AAMI, Arlington, VA, 1999.

[46] C.E. Wen, Y. Yamada, K. Shimojima, Y. Chino, H. Hosokawa, M. Mabuchi, Novel titanium foam for bone tissue engineering, J. Mater. Res. 17 (2002) 2633–2639.

[47] B.V. Krishna, S. Bose, A. Bandyopadhyay, Low stiffness porous Ti structures for load-bearing implants, Acta Biomater. 3 (2007) 997–1006.

[48] H.Y. Mi, J.W. Chen, L.H. Geng, B.Y. Chen, X. Jing, X.F. Peng, Formation of nanoscale pores in shish-kebab structured isotactic polypropylene by supercritical CO_2 foaming, Mater. Lett. 167 (2016) 274–277.

[49] H.Y. Mi, X. Jing, M.R. Salick, T.M. Cordie, X.F. Peng, L.S. Turng, Morphology, mechanical properties, and mineralization of rigid thermoplastic polyurethane/hydroxyapatite scaffolds for bone tissue applications: effects of fabrication approaches and hydroxyapatite size, J. Mater. Sci. 49 (2014) 2324–2337.

[50] Y. Li, C. Wen, D. Mushahary, R. Sravanthi, N. Harishankar, G. Pande, P. Hodgson, Mg-Zr-Sr alloys as biodegradable implant materials, Acta Biomater. 8 (2012) 3177–3188.

[51] R.T. Franceschi, B.S. Iyer, Y. Cui, Effects of ascorbic acid on collagen matrix formation and osteoblast differentiation in murine MC3T3-E1 cells, J. Bone Miner. Res. (1994) 843–854.

[52] G.S. Stein, J.B. Lian, T.A. Owen, Relationship of cell growth to the regulation of tissue-specific gene expression during osteoblast differentiation, FASEB J. 4 (1990) 3111–3123.

[53] R.T. Franceschi, B.S. Iyer, Relationship between collagen synthesis and expression of the osteoblast phenotype in MC3T3-E1 cells, J. Bone Miner. Res. 7 (1992) 235–246.

[54] H. Gülsoy, N. Gülsoy, R. Calışıcı, Particle morphology influence on mechanical and biocompatibility properties of injection molded Ti alloy powder, Biomed. Mater. Eng. 24 (2014) 1861–1873.

[55] D.M. Zhang, C.S. Wong, C.E. Wen, Y.C. Li, Cellular responses of osteoblast-like cells to 17 elemental metals, J. Biomed. Mater. Res. A 105 (1) 148–158.

[56] R. Banerjee, S. Nag, J. Stechschulte, H.L. Freaer, Strengthening mechanisms in Ti-Nb-Zr-Ta and Ti-Mo-Zr-Fe orthopaedic alloys, Biomaterials 25 (2004) 3413–3419.

[57] V.S. Saji, C.C. Han, Electrochemical corrosion behaviour of nanotubular Ti-13Nb-13Zr alloy in Ringer's solution, Corros. Sci. 51 (2009) 1658–1663.

[58] Q.L. Loh, C. Choong, Three-dimensional scaffolds for tissue engineering applications: role of porosity and pore size, Tissue Eng. Part. B Rev. 19 (2013) 485–502.

[59] A.M. Vilardell, N. Cinca, N. Garciagiralt, S. Dosta, I.G. Cano, X. Nogués, J.M. Guilemany, Functionalized coatings by cold spray: an in vitro study of micro- and nanocrystalline hydroxyapatite compared to porous titanium, Mater. Sci. Eng. C 87 (2018) 41–49.

[60] J.I. Rosales-Leal, M.A. Rodríguez-Valverde, G. Mazzaglia, P.J. Ramón-Torregrosa, L. Díaz-Rodrí guez, O. García-Martínez, M. Vallecillo-Capilla, C. Ruiz,

M.A. Cabrerizo-Vílchez, Effect of roughness, wettability and morphology of engineered titanium surfaces on osteoblast-like cell adhesion, Colloid. Surfaces A 365 (2010) 222–229.
[61] X. Jing, H.Y. Mi, X.C. Wang, X.F. Peng, L.S. Turng, Shish-kebab-structured poly(ε-caprolactone) nanofibers hierarchically decorated with chitosan-poly(ε-caprolactone) copolymers for bone tissue engineering, ACS Appl. Mater. Inter. 7 (2015) 6955–6965.
[62] S. Balta, S. Demirkol, M. Unlu, Z. Arslan, T. Celik, Neutrophil to lymphocyte ratio may be predict of mortality in all conditions, Brit. J. Cancer 109 (2013) 31253126.
[63] Y. Okazak, E. Nishimura, H. Nakada, K. Kobayashi, Surface analysis of Ti-15Zr-4Nb-4Ta alloy after implantation in rat tibia, Biomaterials 22 (2001) 599–607.
[64] B. Yin, B.J. Xue, Z.H. Wu, J.G. Ma, K.M. Wang, A novel hybrid 3D-printed titanium scaffold for osteogenesis in a rabbit calvarial defect model, Am. J. Trans. Res. 10 (2018) 474–482.
[65] D.J. Lin, C.C. Chuang, J.H.C. Lin, J.W. Lee, C.P. Ju, H.S. Yin, Bone formation at the surface of low modulus Ti-7.5Mo implants in rabbit femur, Biomaterials 28 (2007) 2582–2589.
[66] P. Majumdar, S.B. Singh, M. Chakraborty, The role of heat treatment on microstructure and mechanical properties of Ti-13Zr-13Nb alloy for biomedical load bearing applications, J. Mech. Behav. Biomed. Mater. 4 (2011) 1132–1144.
[67] J. Li, Z.L. Li, R.L. Li, Y.Y. Shi, H.R. Wang, Y.X. Wang, G. Jin, In vitro and in vivo evaluations of mechanical properties, biocompatibility and osteogenic ability of sintered porous titanium alloy implant, RSC Adv. 8 (2018) 36512–36520.
[68] R. Wauthle, V.D.S. Johan, S. Amin Yavari, J. Van Humbeeck, J.P. Kruth, A.A. Zadpoor, H. Weinans, M. Mulier, J. Schrooten, Additively manufactured porous tantalum implants, Acta Biomater. 14 (2015) 217–225.
[69] H.J. Haugen, M. Monjo, M. Rubert, A. Verket, S.P. Lyngstadaas, J.E. Ellingsen, H.J. Rønold, J.C. Wohlfahrt, Porous ceramic titanium dioxide scaffolds promote bone formation in rabbit peri-implant cortical defect model, Acta Biomater. 9 (2013) 5390–5399.
[70] B. Chang, W. Song, T.X. Han, J. Yan, F.P. Li, L.Z. Zhao, H.C. Kou, Y.M. Zhang, Influence of pore size of porous titanium fabricated by vacuum diffusion bonding of titanium meshes on cell penetration and bone ingrowth, Acta Biomater. 33 (2016) 311–321.
[71] H. Attar, L. Löber, A. Funk, M. Calin, L.C. Zhang, K.G. Prashanth, S. Scudino, Y.S. Zhang, J. Eckert, Mechanical behavior of porous commercially pure Ti and Ti-TiB composite materials manufactured by selective laser melting, Mater. Sci. Eng. A 625 (2015) 350–356.
[72] Q.H. Ran, W.H. Yang, Y. Hu, X.K. Shen, Y.L. Yu, Y. Xiang, K.Y. Cai, Osteogenesis of 3D printed porous Ti6Al4V implants with different pore sizes, J. Mech. Behav. Biomed. Mater. 84 (2018) 1–11.
[73] Y.C. Li, Y.F. Ding, K. Munir, J.X. Lin, M. Brandt, A. Atrens, Y. Xiao, J.R. Kanwar, C.E. Wen, Novel β-Ti35Zr28Nb alloy scaffolds manufactured using selective laser melting for bone implant applications, Acta Biomater. 87 (2019) 273–284.